Proc. Lunar Planet. Sci. Conf. 9th (1978), p. 1209–1233.
Printed in the United States of America

Mineralogy, textures and mode of formation of a hibonite-bearing Allende inclusion

JOHN M. ALLEN[1]*, LAWRENCE GROSSMAN[1,2], ANDREW M. DAVIS[1] and IAN D. HUTCHEON[2]

[1]Department of the Geophysical Sciences and [2]Enrico Fermi Institute
The University of Chicago, Chicago, Illinois 60637

Abstract—The origin of a Type A, hibonite-rich, coarse-grained inclusion is investigated with the electron microprobe and petrographic and scanning electron microscopes. The primary phases are hibonite, rhönite, Ti-Al-pyroxene, spinel, perovskite and melilite. Evidence for the crystallization of the bulk of the primary phases, hibonite and melilite, from a melt is lacking, suggesting that they may have condensed directly from a solar nebular gas instead. Primary phases were intensely altered during a later condensation event which deposited grossular, anorthite, nepheline and wollastonite in veins and cavities. Four or five condensate rims were deposited as successive layers on the outside of the inclusion. From inside to outside, they consist of perovskite + spinel, nepheline + anorthite, Ti-Al-pyroxene + diopside, hedenbergite ± wollastonite ± andradite and, finally, prisms of diopside and hedenbergite with wollastonite and andradite. Reverse zoning in melilite; alteration phases and rim phases, which are not stable condensates from a gas of solar composition; and details of the sequence of rim condensates all suggest that the entire condensation history of this inclusion was interrupted by changes in pressure and/or temperature and/or gas phase composition.

INTRODUCTION

Similarities between the mineralogy and crystallization sequence of coarse-grained, Ca-Al-rich inclusions in Allende, and the calculated condensation sequence from a solar gas have been noted by Larimer and Anders (1970), Marvin *et al.* (1970) and Grossman (1972). On the basis of such work, these inclusions are believed to be the earliest solids to have formed in the solar system. Corundum (Al_2O_3) is predicted by condensation calculations to be the first phase to form from a cooling solar gas, but has never been found. However, hibonite ($2CaO{\cdot}12Al_2O_3$) is sometimes found in Allende inclusions. In the absence of thermochemical data on hibonite and based on the chemical similarity between it and corundum, Grossman (1972) inferred that hibonite instead may have been the earliest phase to condense. We have made a detailed textural and mineralogical study of a hibonite-rich inclusion from Allende. The large amount of hibonite present (~20%) may indicate that the inclusion contains material which formed at the initiation of condensation. The data presented here provide important information on the manner in which the minerals in the inclusion grew and accreted.

*Present address: Department of Geology, University of Toronto, Toronto, Ontario, Canada M5S 1A1.

TECHNIQUES

Discovery and sampling

Microscopic examination of a slab surface of the Allende meteorite revealed a very unusual, coarse-grained, irregularly-shaped inclusion (CG-11), about 7 mm in largest dimension. Orange crystals up to 0.3 mm long make up about 20 vol.% of CG-11 and an X-ray powder pattern showed them to be hibonite. Cavities up to 1 mm across are common. In some of these, long, white fibers of wollastonite could be observed. A distinct rim structure is present on the exterior of the inclusion and also around some smaller, adjacent, apparently separated fragments of the inclusion.

Material from around cavities was selected for SEM mounts and excavated from the slab with stainless steel dental tools. Most of the main portion of the inclusion was then removed. From the resulting powder, small chips were hand-picked for microprobe mounts and other samples were taken for trace element analyses (Davis *et al.*, 1978). The remaining portion of the inclusion was then removed from the slab, and a polished thin section was made for petrographic, microprobe and SEM study.

Analytical methods

Analyses were obtained with an ARL-EMX-SM electron microprobe operated at 15 kV with a focused beam. Using wavelength dispersion, analyses of melilite, hibonite, perovskite and spinel were performed by means of three automated spectrometers driven by an on-line NOVA 2/10 computer. Beam current was 0.3–0.4 μa. The computer program MAGIC (J. W. Colby, Bell Laboratories) was used for matrix corrections.

A Nuclear Semiconductor AUTOTRACE energy-dispersive system on-line with a NOVA 2/10 computer was used for analysis of pyroxenes and fine-grained phases, plus additional analyses of the phases listed above. Data reduction followed closely the procedure outlined by Reed and Ware (1973) using computer programs modified slightly from those supplied by N. Ware. Beam currents of either 0.06 μa or 0.09 μa and counting times of either 1 or 2 minutes were used. Unless otherwise stated, all analytical data discussed in the mineral chemistry section of this paper were obtained by the wavelength-dispersive method.

Fine-grained material in the inclusion was studied with a JEOL JSM-35 scanning electron microscope fitted with a KEVEX Si(Li) X-ray dectector. Phases were identified by visually comparing unknown spectra to spectra of phases analyzed previously by electron microprobe.

TEXTURE AND MINERALOGY

General description

The shape of this inclusion was observed in the plane of the slab surface as well as in the plane of a thin section cut several mm below the slab surface. Not only did the external shape and dimensions of CG-11 change tremendously from one plane to the next, but also what was one inclusion on the slab surface became 3 separate portions in the thin section. The three-dimensional shape of this inclusion is highly irregular.

Examination of CG-11 in polished thin section reveals that it consists of four texturally distinct portions (Fig. 1):

1. A 'coarse-grained' portion consisting of melilite, Ti-Al-pyroxene, perovskite, spinel, hibonite and rhönite.
2. Fine-grained material inferred to be an alteration product of 'coarse-grained' hibonite, melilite and pyroxene, and consisting of grossular, nepheline, anorthite, wollastonite and possible sodalite.
3. A narrow (~50 μm) rim around the exterior of all portions of the inclusion, and consisting of successive layers, from inside to outside, of perovskite + spinel, anorthite + nepheline + voids, Ti-Al-clinopyroxene + diopside and hedenbergite ± wollastonite ± andradite. This rim sequence is identical to that described from Type A inclusions by Wark and Lovering (1977).
4. A discontinuous outer rim up to 300 μm thick, consisting of clinopyroxene needles in the composition range diopside-hedenbergite, plus wollastonite and andradite.

These are listed in order of formation, except for portion two which may post-date the perovskite + spinel rim layer in portion three.

Coarse-grained regions

Point counting of the thin section gives the following modal composition of the coarser, melilite-rich portion, exclusive of fine-grained alteration material: 82% melilite, 6% perovskite, 5% spinel, 4% Ti-Al-pyroxene and 3% hibonite. This inclusion falls into the coarse-grained, Type A category of Grossman (1975) on the basis of the large amount of melilite and the minimal amount of pyroxene present. The observation of a large amount of hibonite on the slab surface in the largest portion of the inclusion, most of which was removed prior to thin sectioning, suggests that the modal composition measured in thin section is not representative of the entire inclusion.

Melilite crystals are up to 200 μm in longest dimension, and tabular on (001). Many are intensely shocked with abundant shock lamellae perpendicular to (001), and grains may be bent through 90°. All show signs of extensive alteration in varying degrees in the form of corrosion and replacement by fine-grained grossular, nepheline and anorthite along grain boundaries, cleavage planes and fractures (Fig. 1b). Alteration is so intense that melilite-melilite grain contacts are rarely observed. Where such contacts can be seen, however, they are curved or linear, without intervening voids or fine-grained phases, indicating that the melilite crystals once formed a compact, interlocking mass making up the bulk of the inclusion prior to corrosion and alteration.

Included in melilite are minor amounts of perovskite (≤30 μm), spinel (≤10 μm), Ti-Al-pyroxene (≤30 μm), and fine needles of an as yet unidentified prismatic mineral (≤10 μm). Perovskite occurs as multifaceted crystals, either as

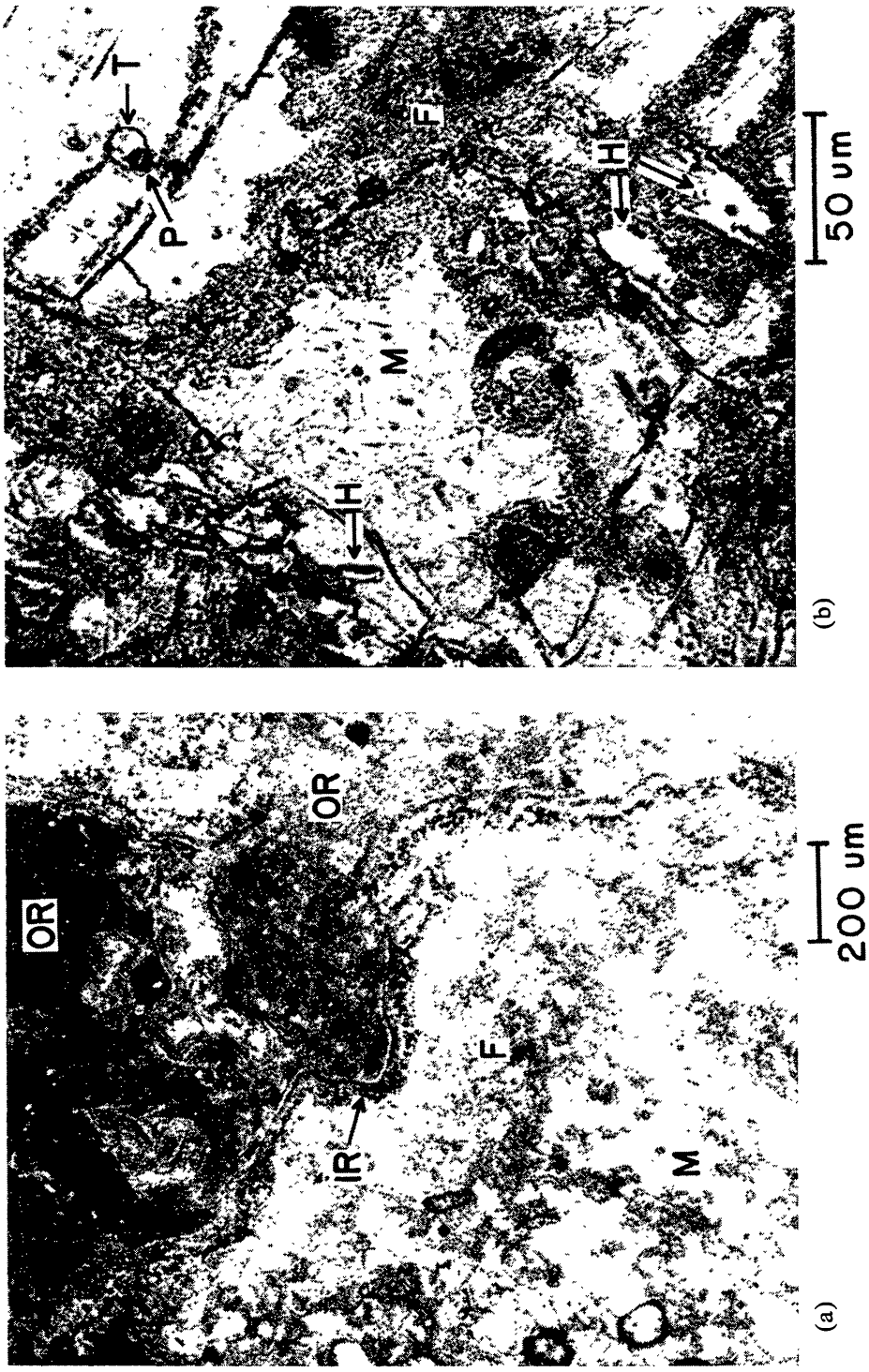

Fig. 1 (a). Part of Allende inclusion CG-11 (transmitted light). Melilite (M) partly altered to fine-grained phases (F). A narrow inner rim (IR) and thick outer rim (OR) surround the main mass of the inclusion, as well as several separate portions (upper right). (b). Melilite partially replaced by fine-grained grossular, nepheline and anorthite (F). Perovskite (P) is rimmed with Ti-Al-pyroxene (T). Hibonite (H) is enclosed by fine-grained phases (lower right) and melilite (left).

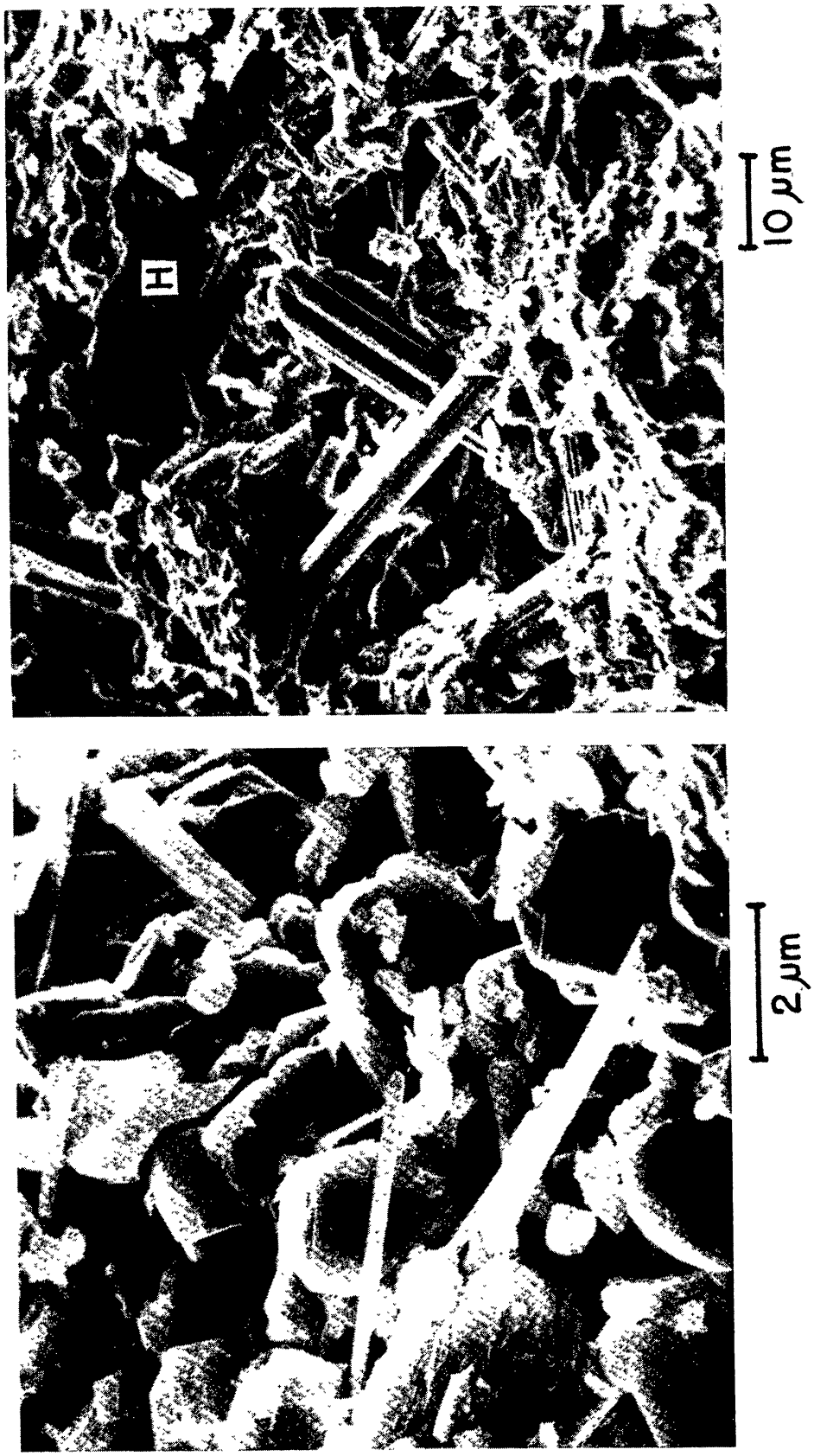

Fig. 1 (c). Euhedral grossular crystals in a cavity from inside (CG-11). The needles are wollastonite. (d). Striated nepheline needles growing on hibonite.

isolated grains in melilite, or rimmed with Ti-Al-pyroxene, or associated with spinel. Pyroxene rimming perovskite (Fig. 1b) only partially encloses the perovskite and is rounded without crystal faces or shows indistinct crystal form with rounded corners. The rimming relationship suggests that the pyroxene grew after the perovskite. Whether the pyroxene is older than the melilite or a later reaction product between melilite and perovskite cannot be determined unambiguously from the textures alone. Spinel associated with perovskite occurs as rounded grains but there is no obvious rimming relationship between them. In addition to these occurrences, Ti-Al-pyroxene and spinel are both found as isolated grains in melilite, in the form of rounded prisms and octahedra, respectively. Ti-Al-pyroxene also occurs as large (up to 110 μm) prisms between melilite grains.

Hibonite occurs as ragged, elongate crystals between melilite grains where it is always surrounded by fine-grained material (Fig. 1b). Often a number of adjacent hibonites such as those in Fig. 1b have the same optical orientation, suggesting they were once part of the same much larger grain. These grains may have originally been 80 μm or more in size but have been severely corroded and replaced by fine-grained material. This hibonite has wavy extinction, perhaps indicative of strain due to shock effects. Hibonite is completely free of inclusions of other phases, but itself may occasionally occur as tiny (<10 μm), rounded, elongate grains in melilite, suggesting that hibonite crystallized before melilite.

Rhönite is rare and occurs as unaltered inclusions in melilite. Fine needles of a colorless, prismatic mineral with approximately square cross-section occur sparsely in melilite. The mineral has a refractive index similar to, or higher than, pyroxene and is frequently oriented either parallel or perpendicular to the (001) cleavage of the enclosing melilite. It is, therefore, probably an exsolution or alteration product of melilite, and also has been observed by us in other coarse-grained Allende inclusions.

Several noble metal-rich alloy nuggets up to 0.3 μm in size were observed with the SEM. These bodies are in contact with the surface of a hibonite crystal and may be partially embedded in it, but are surrounded largely by fine-grained alteration products, mainly grossular. The nuggets consist largely of a Pt, Fe, Ni, Os, Ir, Ru, Rh alloy in which are embedded smaller grains of a Ru, Os, Ir alloy. These objects are similar to those described by Palme and Wlotzka (1976), Wark and Lovering (1976) and El Goresy *et al.* (1977), but their mode of occurrence, in contact with hibonite, has not been reported previously.

Fine-grained alteration products

Point-counting shows that 77% of the inclusion, exclusive of rim material, consists of fine-grained phases and that coarse-grained melilite, Ti-Al-pyroxene and hibonite now make up only 23% of the inclusion. Fine-grained material coats the rounded surfaces of melilite, pyroxene and hibonite grains, fills or partially fills regions between them and penetrates fractures and cleavage planes in melilite. The fine-grained material is thus interpreted as an alteration product of

the coarse-grained primary phases.

Study of thin sections revealed that, in places, veins of fine-grained material pass into cavities which are also lined with fine-grained material. Apart from occasional needles of nepheline and anorthite visible in thin section, much of the fine-grained material cannot be resolved optically. Identification of phases in it was performed with an electron microprobe and an SEM equipped with an energy-dispersive X-ray detector. In addition to the above-mentioned nepheline and anorthite, grossular and possible sodalite were found. The SEM was also used to identify phases in, and study textural features of, fine-grained material in cavities. Here, euhedral grossular crystals, showing mostly trapezohedral and dodecahedral forms, have grown on melilite grains (Fig. 1c). Perched on grossular and projecting into the interiors of cavities are striated prisms of nepheline (Fig. 1d) and beautiful sprays and mats of acicular wollastonite crystals (Fig. 2a,b). Some wollastonite needles are only one μm thick and over 100 μm long. Others are bent through nearly 90°, reminiscent of strong, but flexible, whiskers formed by vapor deposition. The fact that euhedral crystals are separated by, and project into, void spaces indicates that alteration of primary phases, melilite, pyroxene and hibonite, to grossular, nepheline, anorthite and wollastonite occurred in the presence of a vapor phase.

Inner rim

A narrow rim, about 50 μm thick, encloses all portions of CG-11 (Fig. 1a). The sequence of mineral zonation (Fig. 2c) is identical to that found in other Type A inclusions by Wark and Lovering (1977) and will be described only briefly.

The first, or innermost, zone of the rim sequence consists of perovskite and spinel. Textural relationships of this layer are confusing. In places, trains of perovskite and spinel grains pass through relatively unaltered melilites, suggesting their crystallization before melilite in the outer portion of the inclusion and hence before the alteration of melilite to fine-grained material. Elsewhere, the layer appears to overlap fine-grained material in the interior of the inclusion, suggesting either that perovskite and spinel postdate the fine-grained phases present as alteration products of melilite, or that alteration proceeded below the perovskite-spinel layer via cracks. The other zones of the rim consist, from inside to outside, of nepheline + anorthite + voids, Ti-Al-pyroxene + diopside and hedenbergite ± andradite ± wollastonite.

Outer rim

A discontinuous, outer rim up to 300 μm thick adheres to the inner rim at several places on the inclusion (Figs. 1a, 2c). It consists largely of porous, felted masses of clinopyroxene prisms, the latter up to 40 μm in length. Other phases seen in this rim layer are wollastonite, andradite, olivine, pentlandite and Ni-Fe metal. With the exception of metal and sulfide, these are all minerals found in

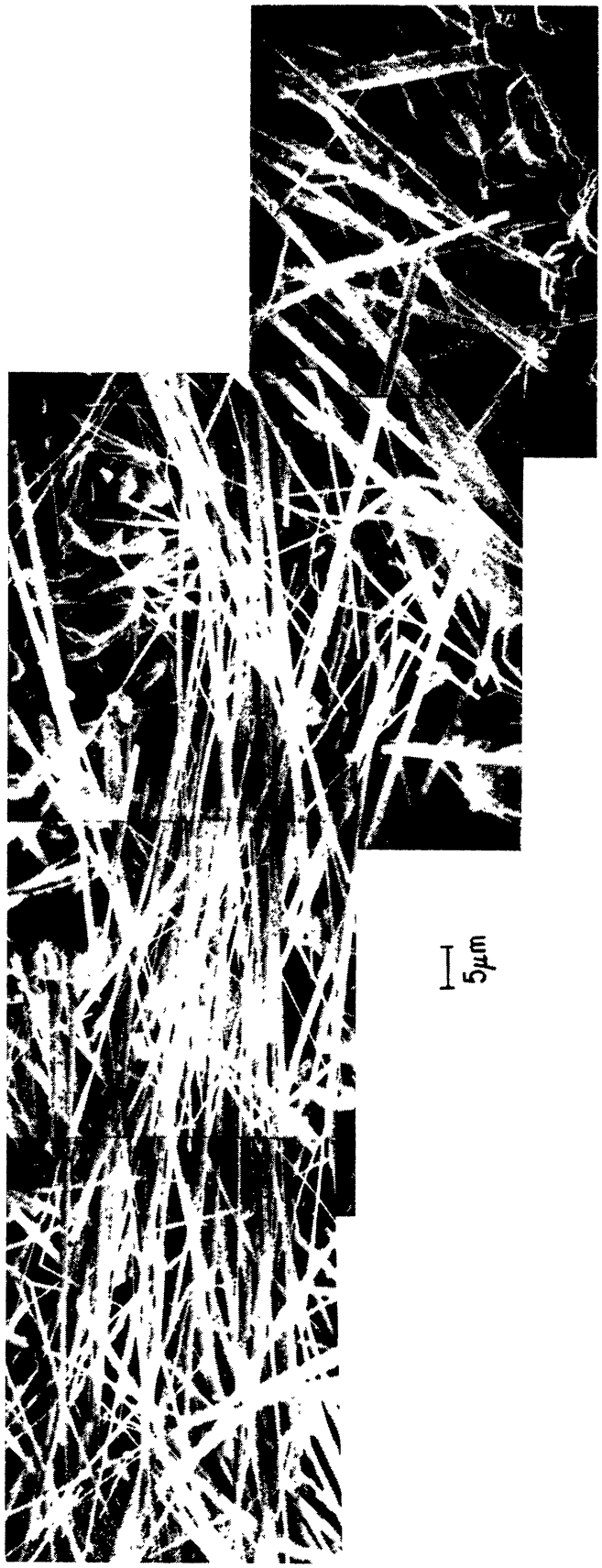

Fig. 2. (a) Sprays of wollastonite needles growing on grossular. Note the needle bent through 90° (middle right). (b) A cavity in melilite, in which are growing euhedral grossular crystals and wollastonite needles. (c) The rim region of CG-11. Melilite partly replaced by grossular (G), nepheline (N) and anorthite (A) makes up the interior of the inclusion. The rim consists, from left to right, of thin layers of perovskite + spinel, nepheline + anorthite + voids (V), Ti-Al-pyroxene + diopside (T), hedenbergite (Hd), and a thick layer of clinopyroxene grains (Cpx) and voids.

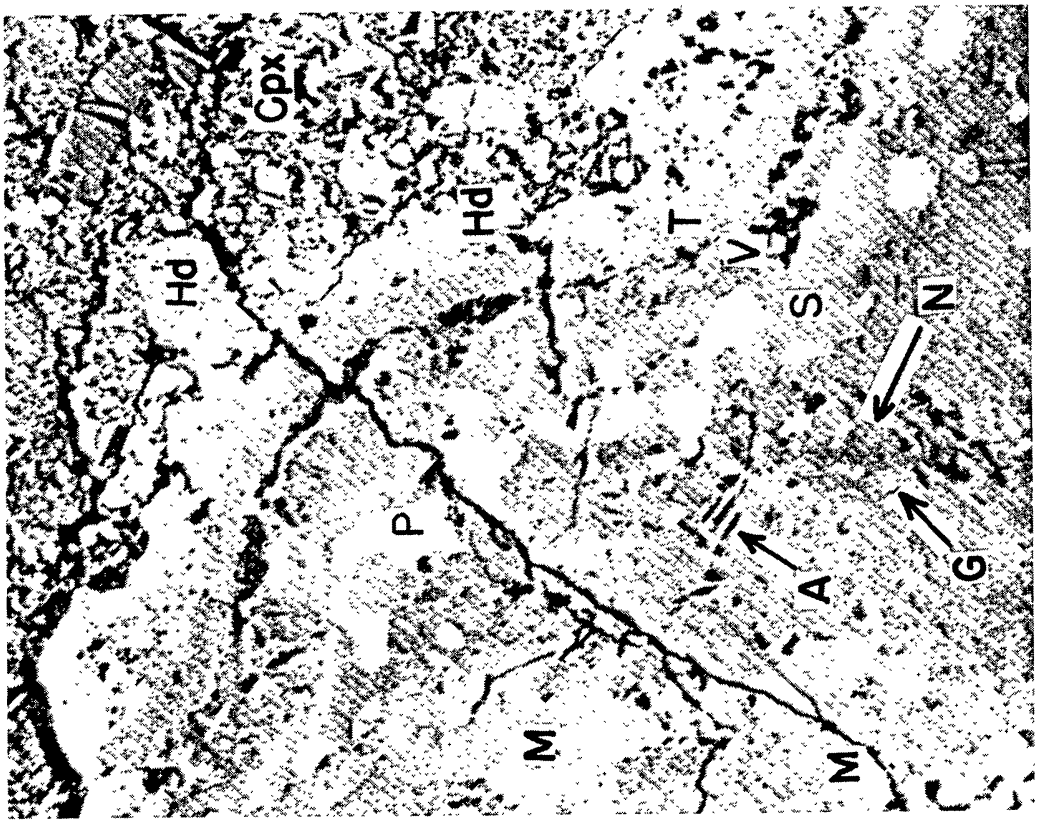

the two outer zones of the inner rim. We have also observed zoned fragments of rafted inner rim material in this region, so that it clearly accreted on the inclusion after the inner rim layers were formed.

Adjacent to the main mass of CG-11 are several smaller objects (Fig. 1a) with identical mineralogy, implying that they are all pieces of the same inclusion. The inner rim sequence completely encloses each piece, and all pieces are embedded in, and connected to the main mass, by a region of outer rim material. Either these are physically separate pieces of the inclusion or they are interconnected in three dimensions. In either case the shape of the inclusion is highly irregular. Wark and Lovering (1977) argued that rimming occurred prior to incorporation in the meteorite parent body, which suggests that the irregular form of the inclusion was also acquired prior to incorporation. The outer rim material may have acted as a cement holding the portions of the inclusion together prior to incorporation.

This pyroxene-rich rim material was searched for in ten Allende thin sections and only found in one, adjacent to a Type B coarse-grained inclusion. Apparently, this material entered the Allende meteorite attached to the outsides of some inclusions.

MINERAL CHEMISTRY

Melilite

Melilite was analyzed using wavelength-dispersive techniques. As found by Grossman (1975), compositions are essentially pure solid solutions between gehlenite ($Ca_2Al_2SiO_7$) and åkermanite ($Ca_2MgSi_2O_7$). Minor element abundances are below the detection limit in the majority of analyses: K_2O <0.02%, Na_2O <0.03%, FeO <0.06%, TiO_2 <0.05%.

Melilite ranges in composition from $Åk_0$ to $Åk_{20}$, with a mean of $Åk_8$ (Fig. 3). This is at the low-Åk end of the range encountered in 16 Type A inclusions from Allende by Grossman (1975). Since condensation theory (Grossman, 1972) and crystal-liquid equilibria for Åk <72 (Osborn and Schairer, 1941) both indicate that melilites on the Åk-Ge join become more åkermanite-rich with falling temperature, it can be inferred that CG-11 crystallized at higher temperature than did the majority of Type A inclusions, consistent with its relatively large ratio of hibonite to spinel. Individual melilite crystals have ranges of composition spanning most of the range observed for the whole inclusion. They are zoned in a somewhat irregular fashion (Fig. 4), from cores of high Åk to rims of low Åk; that is, with decreasing Mg and Si and increasing Al towards the rim. One crystal was analyzed in detail by the energy-dispersive method with analyses performed at 4 μm intervals along five traverses across the crystal. Compositions range from $Åk_{17}$ in the core to $Åk_3$ in the rim. Traverses across fine-grained alteration material in fractures show no systematic or symmetrical compositional gradients about the alteration zones (Fig. 4). Furthermore, compositional contours are transected by fine-grained material at the margins of the grain. We

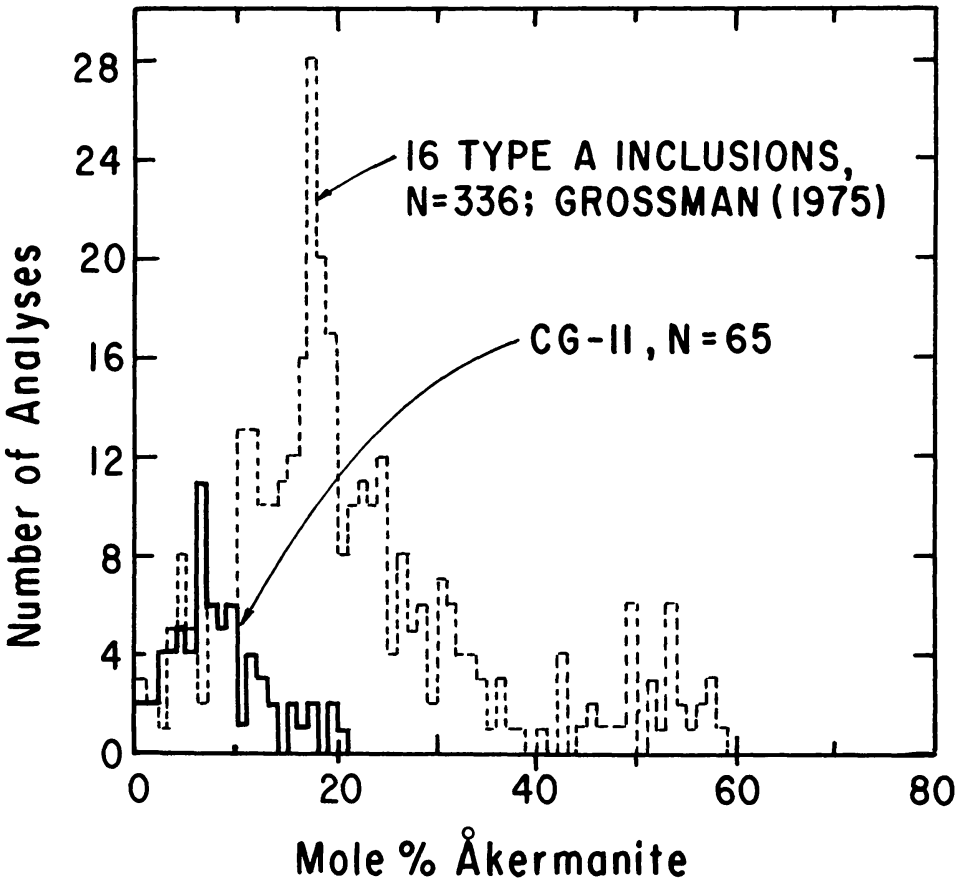

Fig. 3. Melilite composition histogram for the Allende inclusion CG-11, compared to the histogram for 16 Type A inclusions in Allende from Grossman (1975). Melilite in CG-11 is richer in the åkermanite component than is the melilite in most Type A inclusions.

conclude that the crystal was once larger in size prior to alteration and that the alteration process has not changed the major element composition of the melilite in any way; that is, the zoning pattern is a prealteration feature. The direction of zoning in melilite is reversed from what would be expected had it condensed from a vapor or crystallized from a liquid with falling temperature (P constant). Reverse zoning could, however, be produced by a change in composition of the medium from which the crystal grew, and/or an increase in T or decrease in P. In these zoning profiles, the Mg content tends to drop steeply and then level off toward the outer edges of the crystal, resembling an overgrowth. This suggests that conditions changed during growth of the crystal, rather than after.

Traverse C-D (Fig. 4) passes over a Ti-Al-pyroxene rim on perovskite. Because the Al/Mg ratio of the pyroxene is 8 and that of the adjacent melilite is 20, the lack of a detectable compositional gradient in melilite towards the pyroxene indicates that no reaction relationship exists between the pyroxene, melilite and perovskite. The perovskite and pyroxene evidently formed a composite grain which was incorporated in later-formed melilite.

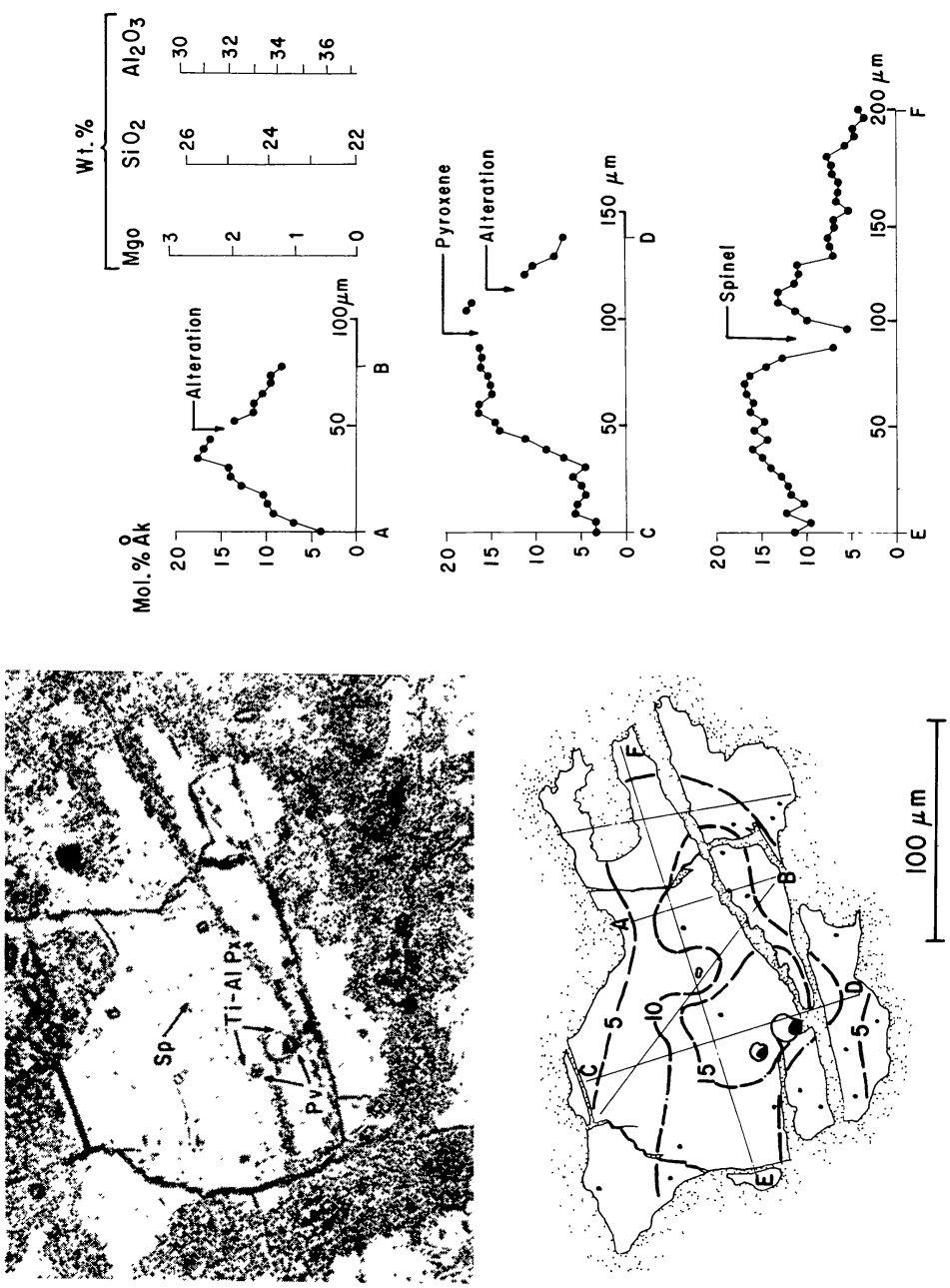

Fig. 4. Analyzed melilite grain (left) in CG-11. Inclusions are spinel, and perovskite rimmed with Ti-Al-pyroxene. Fine-grained grossular, nepheline, and anorthite mantle melilite and replace it along fractures. Sketch shows analyzed spots (dots) and traverses along which analyses were performed (right). Contours at 5, 10, 15 mole percent of the åkermanite component.

1978LPSC....9.1209A

Table 1. Analyses of hibonite, perovskite, and spinel from the Allende coarse-grained inclusion, CG-11.

	Hibonite			Spinel				Perovskite			
				Interior		Rim		Interior		Rim	
MgO	3.53	3.73	4.23	28.45	28.16	24.04	23.65	0.05	0.04	0.05	0.06
Al_2O_3	79.21	78.91	75.75	70.90	68.94	66.67	66.94	0.34	0.38	0.48	0.35
SiO_2	0.43	0.29	0.35	0.26	0.10	0.14	0.15	0.38	0.22	0.24	0.12
CaO	8.82	8.25	8.26	0.12	0.32	0.20	0.35	41.37	40.86	41.09	40.50
Sc_2O_3	0.14	0.12	0.10	<0.02	<0.02	<0.02	<0.02	0.10	0.20	0.16	0.15
TiO_2	6.78	7.19	8.30	0.31	0.19	0.41	0.36	58.15	58.23	57.56	57.91
V_2O_3	0.31	0.37	0.47	0.30	1.20	0.37	0.43	n.d.	n.d.	n.d.	n.d.
Cr_2O_3	<0.07	<0.07	<0.07	0.34	0.08	0.15	<0.05	<0.07	0.14	<0.07	<0.07
FeO	0.05	0.07	0.28	0.07	0.09	6.50	6.34	0.06	0.09	0.16	0.19
Y_2O_3	<0.03	<0.03	<0.03	<0.02	<0.02	<0.02	<0.02	0.17	0.35	0.14	0.28
ZrO_2	n.d.	n.d.	n.d.	<0.02	<0.02	<0.02	<0.02	0.26	0.43	0.43	0.11
Total	99.27	98.93	97.74	100.75	99.08	98.48	98.22	100.88	100.94	100.31	99.67
	Cations per 38 oxygens			Cations per 32 oxygens				Cations per 6 oxygens			
Mg	1.200	1.274	1.469	7.998	8.079	7.130	7.025	0.003	0.003	0.003	0.004
Al	21.326	21.298	20.793	15.763	15.641	15.636	15.720	0.018	0.020	0.026	0.018
Si	0.097	0.067	0.080	0.048	0.018	0.028	0.030	0.017	0.009	0.011	0.005
Ca	2.158	2.025	2.061	0.025	0.066	0.042	0.075	1.987	1.964	1.988	1.971
Sc	0.027	0.024	0.021	—	—	—	—	0.004	0.007	0.006	0.006
Ti	1.165	1.237	1.454	0.044	0.028	0.061	0.054	1.960	1.965	1.954	1.978
V	0.057	0.067	0.088	0.045	0.185	0.059	0.069	—	—	—	—
Cr	—	—	—	0.051	0.012	0.023	—	—	0.005	—	—
Fe	0.008	0.014	0.054	0.012	0.015	1.081	1.056	0.002	0.003	0.006	0.007
Y	—	—	—	—	—	—	—	0.004	0.008	0.003	0.006
Zr	—	—	—	—	—	—	—	0.006	0.009	0.009	0.002
Σ	26.038	26.006	26.020	23.986	24.044	24.060	24.029	4.001	3.993	4.006	3.997

n.d. = not determined due to peak interferences.

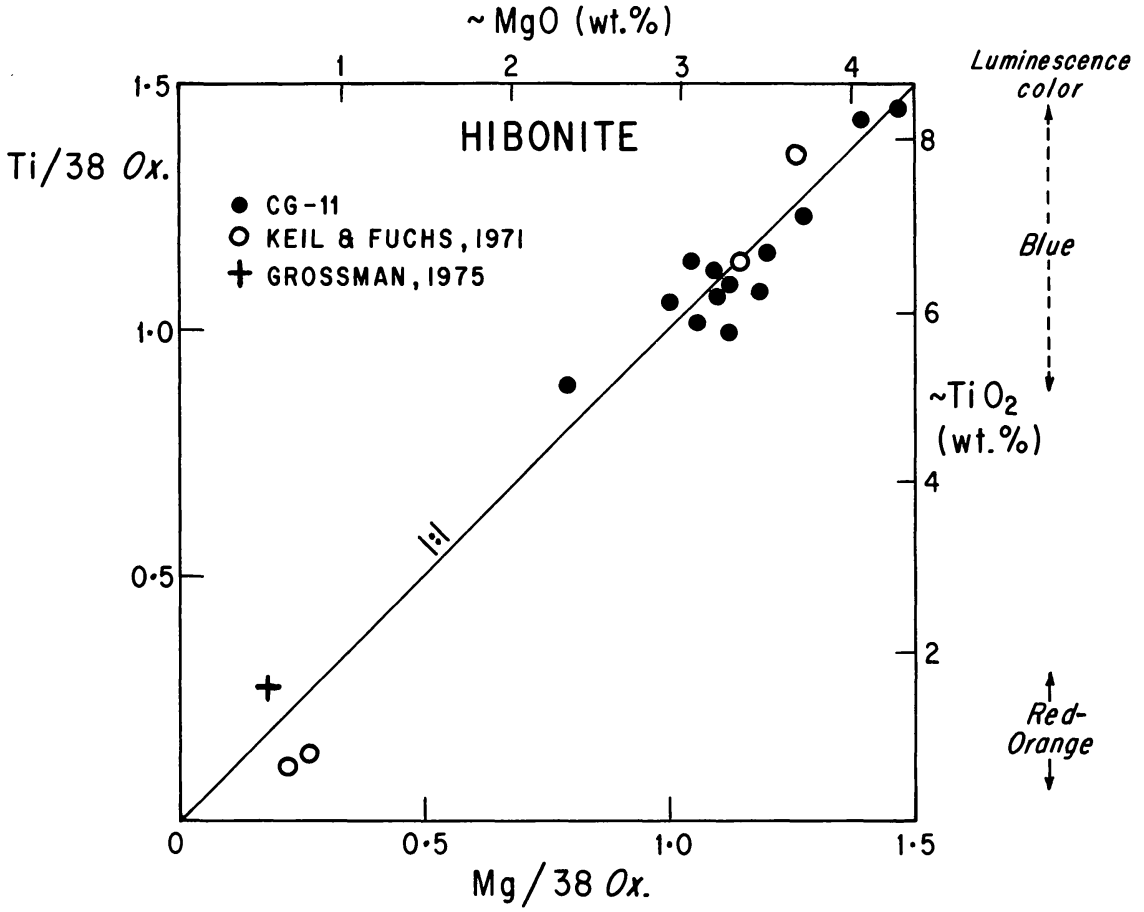

Fig. 5. Ti (total titanium as Ti^{4+}) versus Mg in hibonite from CG-11. Analyses of hibonite from one other Type A inclusion (Grossman, 1975), and from Allende and Leoville (Keil and Fuchs, 1971) are also plotted. Points are close to the 1:1 correlation line.

Traverse E-F passes over a tiny spinel grain. In this case, the melilite is symmetrically zoned about the spinel, with the shapes of the compositional curves (Fig. 4) approximating an exponential diffusion gradient. This can be interpreted as resulting from reaction between spinel and melilite. Equilibrium condensation calculations (Grossman, 1972) predict that gehlenitic melilite reacts with a gas of solar composition on cooling to produce spinel and a more åkermanite-rich melilite. Therefore, when a spinel crystal grows inside a melilite grain, the melilite adjacent to the spinel is expected to become more åkermanitic. The opposite is the case here. We deduce that the observed zonation is a result of reaction between melilite and spinel to produce more gehlenitic melilite and gas; such a reaction taking place in response to an increase in temperature, and/or a decrease in pressure, and/or a change in composition of the gas phase. This is compatible with the reverse zoning of the melilite grains in CG-11 which could be produced in a similar fashion. That spinel has been partially resorbed in this process is suggested also by the rounded form of the spinel grains inside melilite.

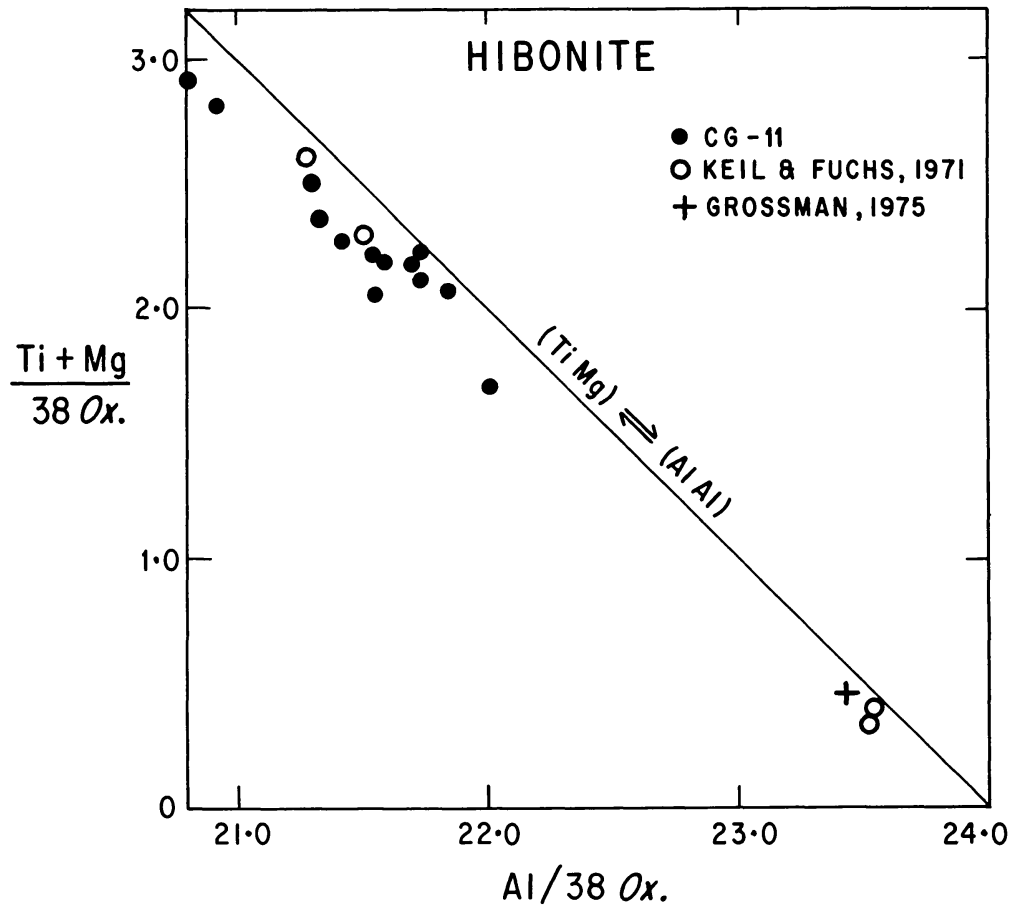

Fig. 6. Ti (total titanium as Ti^{4+}) plus Mg versus Al in hibonite. Same analyses as in Fig. 5. Points fall just below a line for the substitution $(Ti^{4+}Mg) \rightleftarrows (Al\ Al)$.

Hibonite

Hibonite is the high-Mg variety (2.4–4.1% MgO) and luminesces blue (Table 1; Fig. 5). A plot of Ti (total Ti as Ti^{4+}) versus Mg of hibonite analyses from this work and that of Keil and Fuchs (1971) and Grossman (1975) shows a good 1:1 correlation between cation proportions, suggesting crystal-chemical constraints on their substitution in the hibonite structure. A plot of Ti + Mg versus Al (Fig. 6) shows that analyses plot slightly below a line for the coupled substitution $(Ti^{4+}Mg^{2+}) \rightleftarrows (Al^{3+}Al^{3+})$. Hibonite in CG-11 contains 0.11–0.16 (mean 0.13)% Sc_2O_3 and 0.32–0.41 (mean 0.35)% V_2O_3. The concentration levels of these elements are sufficiently high to account for the deviation of the points from the line in Fig. 6. With total Ti calculated as Ti^{4+}, the cation sums in all analyses, Table 1, are close to 26 per 38 oxygens, indicating that little Ti^{3+} is present. Furthermore, if significant Ti^{3+} were present, there would be no coupled substitution of Ti^{3+} with Mg^{2+}, and the 1:1 relationship of Ti with Mg would not be present. Most of the Ti in hibonite must therefore be present as Ti^{4+}.

Other minor elements searched for, but not detected in hibonite, and their

detection limits (weight percent of the element) are Cr(0.05), Y(0.02), Nb(0.03), Ce(0.03), Nd(0.03), Gd(0.04), Dy(0.05), Ho(0.02), Er(0.02).

Perovskite

As seen in Table 1, perovskite is nearly pure $CaTiO_3$. Minor elements detected are 0.06–0.39 (mean 0.16)% Sc_2O_3, 0.03–0.19 (mean 0.12)% FeO, 0.11–0.43 (mean 0.31)% ZrO_2, 0.06–0.35 (mean 0.15)% Y_2O_3 and 0.14% Cr_2O_3 in one perovskite (<0.07 in all other analyses). Data for V_2O_3 are uncertain due to interference from Ti(Kβ), but we estimate that 0.12% V_2O_3 is present. Perovskites in the rim are richer in iron (0.14–0.19% FeO) and poorer in yttrium (0.06–0.28% Y_2O_3) than those included in melilite (0.03–0.09% FeO, 0.14–0.35% Y_2O_3).

Minor elements searched for, but not detected in perovskite, and their detection limits (weight percent of the element) are Nb(0.04), Ce(0.04), Nd(0.03), Gd(0.05), Dy(0.06), Ho(0.02) and Er(0.02).

Spinel

Spinels included in melilite in the interior of the inclusion are iron-poor (0.07–0.17% FeO), whereas those in the rim are iron-rich (6.34–6.97% FeO). In addition, spinels in the interior are generally richer in vanadium (0.25–1.20% V_2O_3) and chromium (0.05–0.34% Cr_2O_3) than those in the rim (0.37–0.43% V_2O_3, ≤0.15% Cr_2O_3). Those in the rim, in addition to being enriched in iron, are also richer in titanium (0.36–0.42% TiO_2) than spinels in the interior (0.19–0.36% TiO_2).

Pyroxenes

All pyroxenes were analyzed by energy-dispersive techniques (Table 2). Pyroxenes in the interior of the inclusion, judged to be of primary origin on the basis of textural and compositional relationships described in previous sections, are richer in Al and Ti than rim pyroxenes (Fig. 7). Among the interior pyroxenes are small differences in composition depending on their textural relationships with other phases. Those rimming perovskite are the richest in aluminum (~24% Al_2O_3) and poorest in titanium (~11% TiO_2) of the interior pyroxenes and are unusual in that they contain 1.3–1.7% V_2O_3. Those which occur either as tiny isolated crystals included in melilite, or as larger grains between melilite, are richer in Ti and poorer in Al. On a conventional $CaSiO_3$-$MgSiO_3$-$FeSiO_3$ pyroxene plot (Fig. 8), all these pyroxenes plot along the Wo-En join close to $CaSiO_3$ owing to their high Al and Ti contents and low Mg and Fe contents.

Pyroxenes from the inner rim sequence show a progressive change in composition towards the exterior of the inclusion, from Ti-Al-pyroxene to Al-diopside, to compositions intermediate between diopside and hedenbergite, and finally to a

Table 2. Major element analyses of pyroxenes in CG-11. All analyses performed by energy-dispersive techniques.

	Ti-Al-px in interior			Inner Rim				Outer Rim		
	Rim on perovskite	Between mel. grains	Inclusion in melilite	Ti-Al-px	Ti-Al-px	Al-diop	Heden.	Salite	Fe-salite	Heden.
SiO_2	28.12	30.76	33.34	37.65	46.43	52.38	47.60	49.68	48.56	45.41
TiO_2	10.97	14.81	15.33	9.41	3.42	0.98	—	—	—	—
Al_2O_3	22.08	23.90	19.46	18.12	8.99	3.98	—	2.79	1.18	—
V_2O_3	1.27	—	—	—	—	—	—	—	—	—
CaO	25.88	24.77	25.31	25.40	24.93	25.76	24.51	24.17	23.25	23.06
MgO	2.56	6.48	6.81	9.33	14.10	16.97	0.32	10.66	4.83	—
FeO	—	—	—	—	0.82	0.50	25.77	10.61	20.55	27.90
Total	90.88	100.72	100.25	99.91	98.69	100.57	98.20	97.91	98.37	96.37
				Cations per 6 oxygens						
Si	1.17	1.14	1.24	1.39	1.72	1.89	1.99	1.92	1.96	1.96
Al	1.08	1.04	0.85	0.79	0.39	0.17	—	0.13	0.06	—
Ti	0.34	0.41	0.43	0.26	0.10	0.03	—	—	—	—
V	0.04	—	—	—	—	—	—	—	—	—
Ca	1.15	0.98	1.01	1.00	0.99	0.99	1.10	1.00	1.01	1.07
Mg	0.16	0.36	0.38	0.51	0.78	0.91	0.02	0.62	0.29	—
Fe	—	—	—	—	0.03	0.02	0.90	0.34	0.69	1.01
Σ	3.94	3.93	3.91	3.95	4.01	4.01	4.01	4.01	4.01	4.04

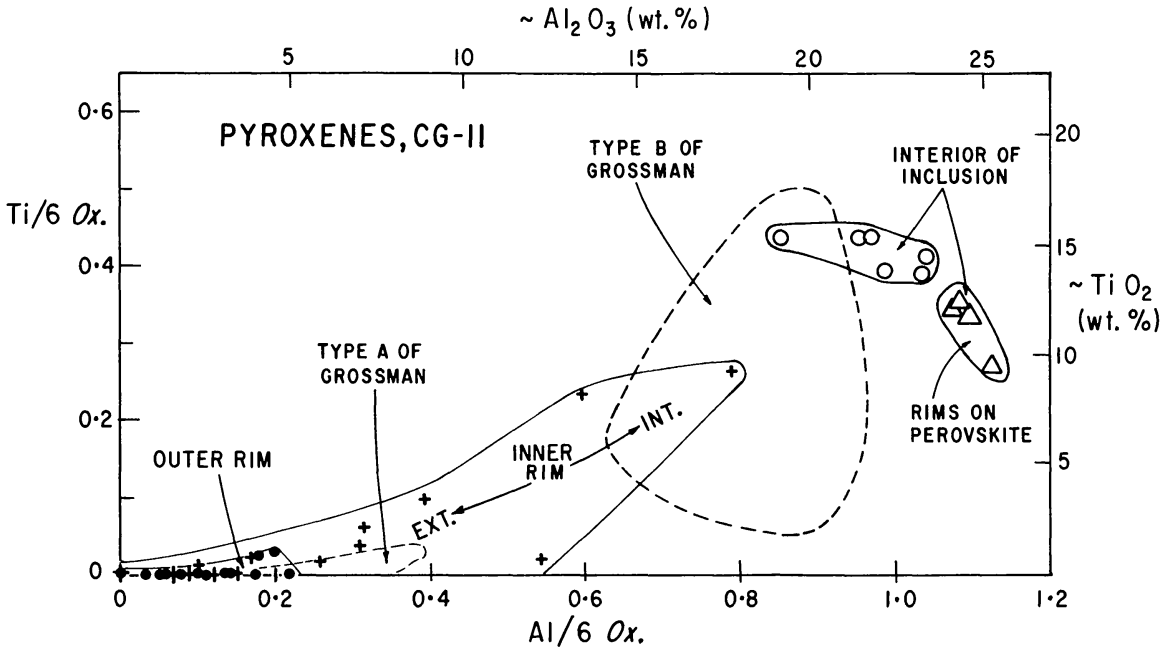

Fig. 7. Ti (total titanium as Ti^{4+}) versus Al in pyroxenes from CG-11. There is a progressive decrease in Ti and Al from pyroxene in the interior of the inclusion, through the inner rim, to the outer rim. The total range of pyroxene composition found in CG-11 is greater than that found in the interiors of a number of Type A and B inclusions (dashed areas) by Grossman (1975).

Table 3. Major element analyses of minerals in the fine-grained portions of CG-11. All analyses performed by energy-dispersive techniques.

	Wollastonite	Grossular	Andradite	Nepheline	Anorthite
SiO_2	48.27	38.62	38.35	41.29	39.18
Al_2O_3	—	24.00	—	34.80	37.05
FeO	0.48	—	26.88*	—	—
MgO	—	—	1.98	—	—
CaO	48.70	38.48	30.89	3.71	19.68
Na_2O	—	—	—	16.24	0.46
K_2O	—	0.09	—	1.66	—
Total	97.45	101.19	98.10	97.70	96.37
			Numbers of ions		
O	6	12	12	32	32
Si	1.94	2.88	3.22	8.01	7.58
Al	—	2.11	—	7.96	8.45
Fe	0.02	—	1.70*	—	—
Mg	—	—	0.25	—	—
Ca	2.10	3.07	2.78	0.77	4.08
Na	—	—	—	6.11	0.17
K	—	0.01	—	0.41	—

*Total iron as Fe^{3+}.

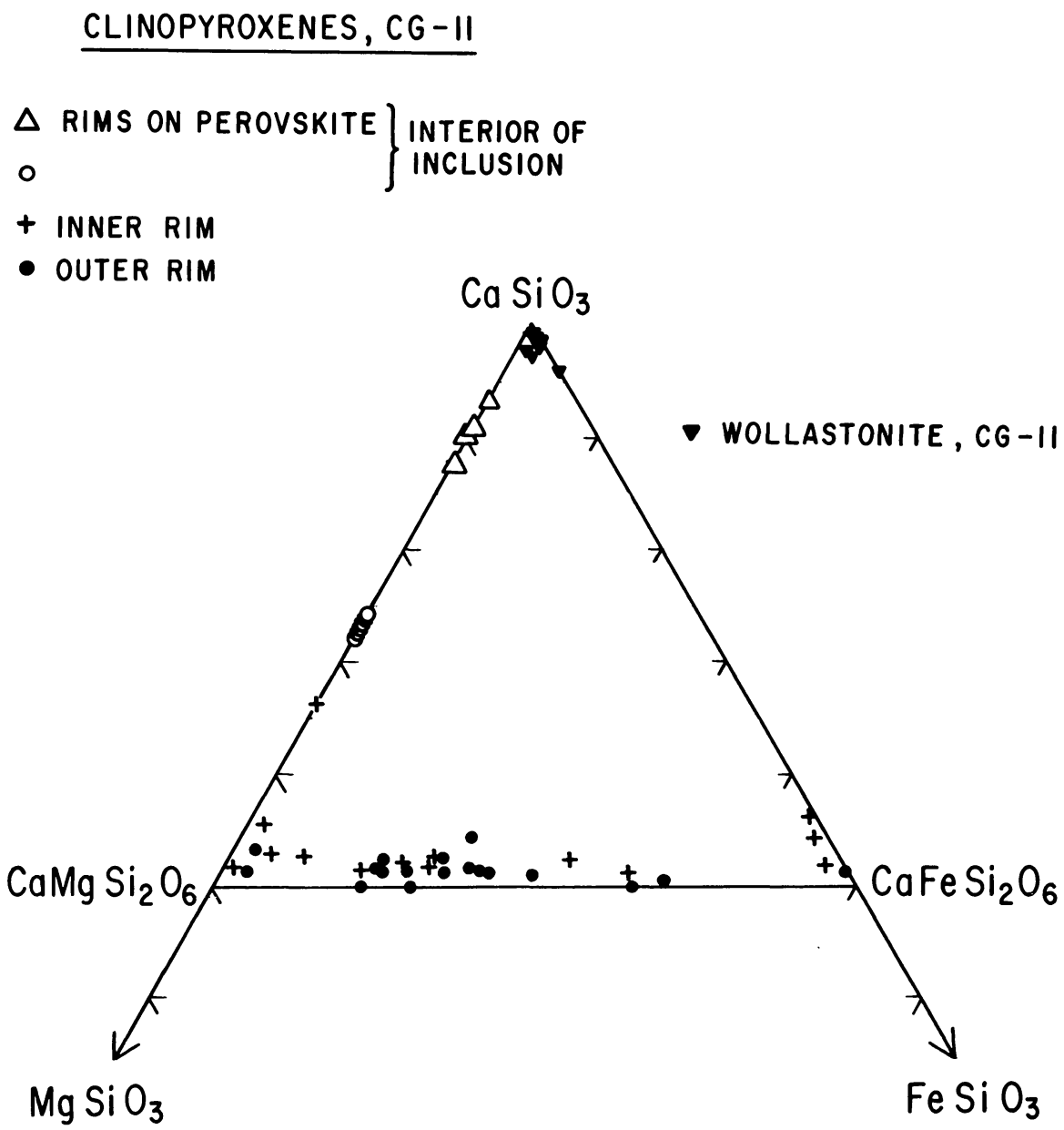

Fig. 8. Pyroxene and wollastonite analyses from CG-11 plotted in terms of the end-members $CaSiO_3$, $MgSiO_3$ and $FeSiO_3$. All pyroxenes lie on or above the diopside-hedenbergite join, and are more Ca-rich than most terrestrial pyroxenes, which plot below the join. Pyroxenes from the interior of the inclusion plot on the Ca-Mg join close to Ca because of Ti and Al substituting for Mg, and their lack of Fe. Pyroxenes of the rim range from diopside to hedenbergite in composition.

layer of pure hedenbergite, as noted by Wark and Lovering (1977) for other Type A inclusions.

The outer, loosely-packed rim zone, which is up to 300 μm thick, consists predominantly of clinopyroxene prisms ranging from diopside with up to 4.6% Al_2O_3 and up to 1.4% TiO_2, to Al- and Ti-free hedenbergite (Figs. 7, 8).

Pyroxenes of different composition are heterogeneously distributed relative to one another and no systematic spatial variation of composition is present. Hedenbergite occurs next to diopside in some places, indicative of extreme disequilibrium.

Haggerty (1977) maintains that Ti^{3+} and $Ti^{3+} + Ti^{4+}$ in condensate pyroxenes should decrease with decreasing crystallization temperature. In the inner rim, increasing Fe/Mg ratios in pyroxene outward must also be due to successively lower crystallization temperatures. If Haggerty is correct, the overall compositional trend from Ti-Al-pyroxene in the interior of the inclusion, through less Ti- and Al-rich rim pyroxene to Al-diopside, to hedenbergite, may be related to condensation at successively lower temperatures. This is supported by the occurrence of significant vanadium, a refractory element (Grossman, 1973), in early-formed, Ti-Al-pyroxenes which rim perovskite in the interior of the inclusion, and its absence from rim pyroxenes.

The range of pyroxene compositions encountered in CG-11, a single inclusion, is greater than that found by Grossman (1975) in a chemical survey of 16 Type A and 9 Type B inclusions from Allende. Furthermore, we find that CG-11, a Type A inclusion, contains 4% of Ti-Al-pyroxene, a variety which Grossman found only in Type B inclusions. A brief survey of several other Type A inclusions studied by Grossman (1975) also revealed the presence of small amounts of a green, Ti-Al-pyroxene, with modes of occurrence and textural relationships similar to those in CG-11. It is emphasized that the major difference between Types A and B inclusions is the high proportion, 35–60%, of Ti-Al-pyroxene in the latter, compared to the former. Our petrographic observations on other thin sections indicate that most, if not all, coarse-grained inclusions probably contain the complete spectrum of pyroxene compositions that are found in CG-11.

Other phases

Several other phases, all fine-grained, were analyzed by energy-dispersive techniques, and representative analyses are shown in Table 3.

The only wollastonite analyzed occurs intergrown with pyroxene in the outer rim. Because of its fine grain size, all analyses have low sums. They show up to 4 mole percent $FeSiO_3$ and up to 2 mole percent $MgSiO_3$ which may either be present in the wollastonite structure or are artifacts produced by excitation of surrounding grains by the microprobe electron beam. In either case, the compositions are fairly close to pure wollastonite (Fig. 8).

In garnet it is assumed that all iron is present as Fe^{3+}, forming the andradite component. Garnets in the fine-grained material in the interior of CG-11 are very close to grossular in composition, with 6 mole percent or less of each of the pyrope and andradite components. Garnets in the rim sequence are iron-rich and close to andradite in composition, with 9% or less pyrope. Andradite in the rim must have crystallized at lower temperatures than did grossular in the interior.

Anorthite analyses show the apparent presence of up to 0.5% Na_2O (Table 3), but this may be an artifact produced from electron excitation of nepheline with

which it is intimately intergrown. Anorthite contains more than 96 mole percent $CaAl_2Si_2O_8$.

Nepheline is Ca-rich (3.7% CaO) and contains about 1.7% K_2O. Analyses are within the compositional range encountered for nephelines in amoeboid olivine aggregates in Allende (Grossman and Steele, 1976).

High chlorine counts in some analyses of fine-grained material from the interior of the inclusion may indicate the presence of sodalite.

Summary and Conclusions

Condensation versus crystallization from a melt

The euhedral form of grossular, nepheline and wollastonite crystals in cavities of CG-11 suggests that these and other fine-grained phases present as alteration products of melilite, hibonite and pyroxene, were deposited from a gas phase. Fine needles of clinopyroxene in the outer rim are separated by void space and were probably deposited from a gas also, and Wark and Lovering (1977) present evidence that the inner rim may have had a similar mode of formation.

Textural relationships of the primary phases (melilite, hibonite, perovskite, spinel and pyroxene) in the interior of the inclusion give no clear indication as to whether they formed from a gas or a liquid. Information bearing on this problem may be obtained by comparing the inferred crystallization sequence of the primary phases with the sequence in a relevant crystal-liquid system. The bulk chemical composition of the primary phases in CG-11 calculated from the mean compositions of the phases and their modal abundances measured in thin section by point-counting is 20% SiO_2, 37% CaO and 35% Al_2O_3, with the rest TiO_2 and MgO. As mentioned previously, the thin section may contain less hibonite than does the bulk of the inclusion. If 20% hibonite is assumed present, the amount estimated crudely from examination of the inclusion on the slab surface, the bulk composition is 16% SiO_2, 31% CaO and 45% Al_2O_3. Neglecting TiO_2 and MgO, which together make up only 8.4–8.6% of the major oxides, we can consider the crystallization of a liquid consisting only of SiO_2, CaO and Al_2O_3 in the proportions determined from the mineralogy of the primary phases in CG-11. In the SiO_2-CaO-Al_2O_3 system (Osborn and Muan, 1960), the calculated bulk composition plots very close to the gehlenite-hibonite join in the primary phase field of gehlenite, even if as much as 20% hibonite is assumed present in the primary assemblage. Equilibrium cooling of melts of these compositions would result in crystallization of gehlenite, followed by co-crystallization of gehlenite and $CaAl_4O_7$, reaction of $CaAl_4O_7$ to form hibonite, co-crystallization of gehlenite and hibonite and then gehlenite, hibonite and anorthite from the final liquid. This crystallization sequence would result in the successive formation of gehlenite crystals containing no inclusions of later-formed phases, gehlenite with inclusions of $CaAl_4O_7$, $CaAl_4O_7$ with inclusions of gehlenite, hibonite with inclusions of gehlenite, gehlenite with inclusions of hibonite and an assemblage of interstitial anorthite, hibonite and gehlenite between crystals of all the earlier-

formed phases. Because all of the hibonite forms either after gehlenite or at the same time as gehlenite, gehlenite inclusions in hibonite should be a very common feature resulting from melts in this composition range.

In CG-11, gehlenitic melilite contains numerous inclusions of earlier-formed perovskite and Ti-Al-pyroxene. Hibonite, on the other hand, occurs largely as isolated grains entirely free of inclusions, suggesting that it formed prior to perovskite, Ti-Al-pyroxene and melilite. This is supported by the rare occurrence of small hibonite crystals in melilite. Thus, the hibonite in CG-11 must have crystallized before melilite. Had these phases crystallized from a melt with the composition of the primary phase assemblage of the inclusion, much of the hibonite would have crystallized after melilite, assuming that the observed amounts of TiO_2 and MgO do not significantly alter the phase relations from those in the system CaO-Al_2O_3-SiO_2.

Assuming that hibonite has similar thermochemical properties to corundum, the observed crystallization sequence of hibonite, followed by perovskite and then melilite more closely follows that predicted by condensation calculations for a gas of solar composition (Grossman, 1972). If this model is accepted, then inclusions of Ti-Al-pyroxene and rhönite in melilite must be interpreted as condensates which formed prior to, or contemporaneously with melilite.

Hibonites, as well as inclusions of pyroxene and spinel in melilite, show small, but significant, variations in composition from grain to grain within the inclusion. Individual hibonites vary in the amount of substitution of Ti and Mg for Al. Pyroxenes rimming perovskite are richer in Al and V and poorer in Ti than those not rimming perovskite. Different spinels have differing V, Cr and Ti contents. Such compositional heterogeneity implies that the grains are not in chemical equilibrium with one another and does not seem reasonable had these grains crystallized from a liquid of uniform composition. Furthermore, had this inclusion crystallized from a melt, we have seen that $CaAl_4O_7$ should have formed during cooling. This phase has not been found in CG-11. Although it could be arged that any $CaAl_4O_7$ which did form should have reacted completely with the liquid on further cooling to form hibonite, the $CaAl_4O_7$ which is predicted to be trapped inside later melilite would have been unable to do so, particularly in view of so much evidence cited here for lack of equilibrium in other phases. It is possible, however, that different grains of hibonite, pyroxene and spinel formed as condensates in gases of slightly differing composition, and/or T, and/or P. These gathered together in one place and were later incorporated by condensing melilite grains.

Finally, had this inclusion crystallized from a melt, it is noted that the last liquid to disappear is expected to form an interstitial assemblage of anorthite plus hibonite plus gehlenite. Although it can be argued that such material may be hidden in the midst of the fine-grained secondary alteration products, no such material is observed in those rare instances where contacts between melilite crystals are preserved, free of alteration products.

Taking all this evidence into account, we believe that the primary phases of CG-11 did not crystallize from an igneous melt.

Physical-chemical conditions during condensation of the inclusion

Textural relationships of minerals in CG-11 indicate a complex sequence of mineral formation processes that cannot be accounted for by simple, monotonic cooling and condensation from a gas of uniform solar composition. The inclusion can be subdivided into four main facies: (1) the earliest-formed or primary region consisting of melilite, hibonite, perovskite, spinel, Ti-Al-pyroxene and rhönite; (2) fine-grained grossular, nepheline, anorthite and wollastonite as alteration products of primary phases; (3) a narrow inner rim sequence on the inclusion, consisting of successive layers, from inside to outside, of perovskite + Fe-spinel, nepheline + anorthite, Ti-Al-pyroxene + diopside and hedenbergite ± andradite ± wollastonite; and (4) a thick, discontinuous outer rim consisting of pyroxene ranging from diopside to hedenbergite in composition, wollastonite, andradite, sulfide and metal.

Textural evidence indicates that melilite was the last to crystallize of the primary phases making up the 'coarse-grained' region of the inclusion. At constant pressure, the åkermanite content of condensing melilite increases with decreasing temperature. At a total pressure of 10^{-3} atm, the most åkermanite-rich melilite in CG-11 ($Åk_{20}$) would have equilibrated with a gas of solar composition at 1480°K (Grossman, 1972). This temperature is, therefore, an approximate lower limit for formation of the primary phases. Condensation may have begun as high as about 1750°K with the formation of hibonite. The reverse zoning in melilite could have taken place in a gas of changing composition or in response to a temporary increase in T or a decrease in P. Formation of the primary phases was followed by an event which severely shocked melilite and hibonite.

Textural relations in the secondary alteration regions show that the alteration products are condensates. Neither grossular nor nepheline nor wollastonite are stable condensates from a gas of solar composition. They may have condensed from a gas of non-solar composition. Alternatively, these phases may be able to condense from a solar gas under non-equilibrium conditions such as those caused by the inability of early-formed condensates to maintain equilibrium with the vapor as it cools. The co-existence of hibonite and spinel in the interior of the inclusion is an indication of this phenomenon, since hibonite, assuming it behaves like corundum, should react completely with a solar nebular gas to form spinel. In either case, grossular, a major component of the alteration assemblage, decomposes above 1100°K, setting an upper limit to the temperature of alteration. This is in accord with the presence of nepheline in the alteration products, since it is unlikely that Na can condense in any form above 1200°K in a gas of solar composition.

Textural relationships indicate that the rim must post-date the formation of most of the melilite and included phases in the interior of the inclusion. The inner rim layer of perovskite and spinel, however, can be seen to pass through melilite grains in less altered portions of the inclusion and to be set back from the outer rim layers in places. Therefore, the perovskite-spinel layer may be contemporaneous with crystallization of melilite in the outer portions of the inclusion.

The rim of the inclusion was formed later than the coarse-grained primary phases in its interior. Whether or not the entire rim sequence post-dates the alteration of the primary phases is not clear on textural grounds, but the fact that primary pyroxenes are altered and rim pyroxenes are not suggests that the latter may be post-alteration in age. Spinel, perovskite and pyroxene in the rim all contain FeO, whereas the same phases in the interior, primary portion of the inclusion do not. Under solar nebular conditions FeO condenses in pyroxene only at low temperatures, below 800°K, and condensation of FeO in the other phases may only be possible at similarly low temperatures. The progressively increasing Fe content of pyroxenes outwards in the rim suggests condensation at successively lower temperatures. An apparent anomaly in the rim sequence is the formation of Ti-Al-pyroxene with very low iron after Fe-spinel, nepheline and anorthite. Fe-bearing spinel and nepheline are probably low-temperature condensates, stable only below 1100°K, whereas, according to Haggerty (1977), Ti-Al-pyroxene may have formed at temperatures above 1350°K. One possible explanation is a brief increase in temperature while the Ti-Al-pyroxene formed. Changes in gas pressure and composition are, of course, also possibilities. This problem has been addressed by Wark and Lovering (1977) who suggested that both core and rim pyroxenes condensed at a lower temperature than nepheline. A logical extension of that idea is the prediction that primary nepheline should coexist with Ti-Al-pyroxenes in the cores of Type B inclusions, a feature that has not been observed.

The outer rim zone of CG-11 consists of individual, loosely-packed crystals of pyroxene ranging from diopside to hedenbergite in composition, plus wollastonite, andradite, olivine, sulfide and metal. Pyroxenes of differing composition are heterogeneously distributed in this zone, as are grains of the other phases. It is probable that the pyroxenes are individual condensate grains which accreted in depressions on the surface of the inclusion. The compositional similarity between the pyroxenes found in the outer and inner rim may indicate that they condensed under similar conditions. Olivine, sulfide and metal grains in the outer rim may be xenoliths of Allende matrix, introduced during compaction of the parent body.

Mineralogical and textural data presented here suggest that all the minerals in CG-11 may have condensed from a gas. The complete lack of equilibrium between some phases and the preservation of high-temperature phases such as hibonite suggest that the inclusion formed rapidly. The compositional variations from grain to grain of hibonite, pyroxene and spinel suggest that each type of grain grew in a slightly different physical-chemical environment. The reverse zoning in melilite can only be explained by variation in composition of the gas from which it grew, or by an increase in T or decrease in P. Wollastonite, grossular and nepheline are not stable in a gas of solar composition, indicating either disequilibrium or non-solar gas composition. We conclude that the minerals in CG-11 condensed from a gas of heterogeneous pressure, and/or temperature, and/or composition, in space and/or time. That hibonite, pyroxene and spinel grains with heterogeneous compositions are gathered together in the

same inclusion, implies movement of grains relative to the gas. Detailed examination by us of other Type A inclusions shows extremely complex textures and mineralogy, similar in many respects of CG-11. All such inclusions may have had a similar, complex mode of formation.

Acknowledgments—We are indebted to Ian M. Steele for helpful advice concerning electron microprobe techniques and to Robert N. Clayton for stimulating discussions. O. Hadfield and M. Bowie typed the manuscript with great alacrity. This work was supported by the National Aeronautics and Space Administration through grants NGR 14-001-249 (Grossman) and NGL 14-001-169 (Clayton) and by funds from the Alfred P. Sloan Foundation and the Louis Block Fund of the University of Chicago. Parts of the research were carried out in the Scanning Electron Microscope Users' Laboratory at the University of Chicago. This laboratory is operated on a resource grant from the National Institutes of Health.

References

Davis A. M., Grossman L. and Allen J. M. (1978) Major and trace element chemistry of separated fragments from a hibonite-bearing Allende inclusion. *Proc. Lunar Planet. Sci. Conf. 9th.* This volume.

El Goresy A., Nagel K., Dominik B. and Ramdohr P. (1977) Fremdlinge: Potential presolar material in Ca-Al-rich inclusions of Allende (abstract). *Meteoritics* **12**, 215–216.

Grossman L. (1972) Condensation in the primitive solar nebula. *Geochim. Cosmochim. Acta* **36**, 597–619.

Grossman L. (1973) Refractory trace elements in Ca-Al-rich inclusions in the Allende meteorite. *Geochim. Cosmochim. Acta* **37**, 1119–1140.

Grossman L. (1975) Petrography and mineral chemistry of Ca-rich inclusions in the Allende meteorite. *Geochim. Cosmochim. Acta* **39**, 433–454.

Grossman L. and Steele I. M. (1976) Amoeboid olivine aggregates in the Allende meteorite. *Geochim. Cosmochim. Acta* **40**, 149–155.

Haggerty S. E. (1977) Refinement of the Ti-cosmothermometer in the Allende meteorite and the significance of a new mineral, $R^{2+}Ti_3O_7$, in association with armalcolite (abstract). In *Lunar Science VIII*, p. 389–391. The Lunar Science Institute, Houston.

Keil K. and Fuchs L. H. (1971) Hibonite $Ca_2(Al,Ti)_{24}O_{38}$ from the Leoville and Allende chondritic meteorites. *Earth Planet. Sci. Lett.* **12**, 184–190.

Larimer J. W. and Anders E. (1970) Chemical fractionations in meteorites—II. Abundance patterns and their interpretation. *Geochim. Cosmochim. Acta* **31**, 1239–1270.

Marvin U. B., Wood J. A. and Dickey J. S. Jr. (1970) Ca-Al rich phases in the Allende meteorite. *Earth Planet. Sci. Lett.* **7**, 346–350.

Osborn E. F. and Muan A. (1960) The system CaO-Al_2O_3-SiO_2. Phase equilibrium diagrams of oxide systems. Published by the American Ceramic Society, Columbus, Ohio.

Osborn E. F. and Schairer J. F. (1941) The ternary system pseudowollastonite-akermanite-gehlenite. *Amer. J. Sci.* **239**, 715–763.

Palme H. and Wlotzka F. (1976) A metal particle from a Ca, Al-rich inclusion from the meteorite Allende, and the condensation of refractory siderophile elements. *Earth Planet. Sci. Lett.* **33**, 45–60.

Reed S. J. B. and Ware N. G. (1973) Quantitative electron microprobe analysis using a lithium drifted silicon detector. *X-Ray Spectrometry* **2**, 69–74.

Wark D. A. and Lovering J. F. (1976) Refractory/platinum metal grains in Allende calcium-aluminium-rich clasts (CARC's): Possible exotic presolar material? (abstract). In *Lunar Science VII*, p. 912–914. The Lunar Science Institute, Houston.

Wark D. A. and Lovering J. F. (1977) Marker events in the early evolution of the solar system: Evidence from rims on Ca-Al-rich inclusions in carbonaceous chondrites. *Proc. Lunar Sci. Conf. 8th*, p. 95–112.